9

Lamina Off-Axis Tensile Response

The off-axis tension test of unidirectional composites has received considerable attention by the composites community. "Off-axis" here refers to the material axes (1-2) being rotated through an angle θ with respect to the specimen axis and direction of loading (Figure 9.1). The off-axis specimen is typically 230 mm long and between 12.7 and 25.4 mm wide. A thickness of eight plies is common (0.127 mm ply thickness).

The off-axis tension test is rarely used to determine basic ply properties. Most commonly, the purpose of this test is to verify material properties determined in tension, compression, and shear, as discussed in Chapters 5–7, using the transformed constitutive relations discussed in Chapter 2. Testing of specimens at off-axis angles between 10 and 20° produces significant shear in the principal material system. Consequently, the 10° off-axis test has been proposed as a simple way to conduct a shear test [1]. The test has been used

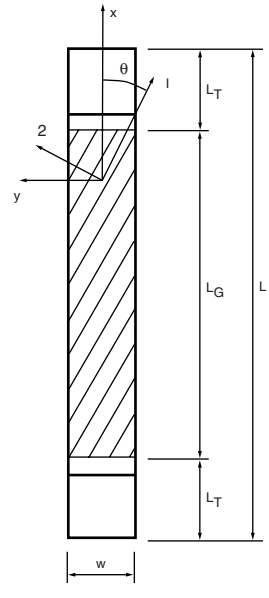

FIGURE 9.1
Geometry of the off-axis tensile coupon.

also to verify biaxial strength criteria because, as will be discussed, uniaxial loading will lead to a combined state of stress in the principal material system.

9.1 Deformation and Stress in an Unconstrained Specimen

Because of the off-axis configuration of the specimen, the in-plane response is characterized by a fully populated compliance matrix, as shown in Equation (2.16)

$$\begin{bmatrix} \varepsilon_x \\ \varepsilon_y \\ \gamma_{xy} \end{bmatrix} = \begin{bmatrix} \bar{S}_{11} & \bar{S}_{12} & \bar{S}_{16} \\ \bar{S}_{12} & \bar{S}_{22} & \bar{S}_{26} \\ \bar{S}_{16} & \bar{S}_{26} & \bar{S}_{66} \end{bmatrix} \begin{bmatrix} \sigma_x \\ \sigma_y \\ \tau_{xy} \end{bmatrix} \tag{9.1}$$

where the x-y system is defined in Figure 9.1, and expressions for the transformed compliance elements $\bar{S}_{ij}$ are given in Appendix A.

For an ideal, uniformly stressed off-axis tensile coupon, the only stress acting is σ_x, ($\sigma_y = \tau_{xy} = 0$), and Equations (9.1) give the state of strain in the specimen,

$$\begin{bmatrix} \varepsilon_x \\ \varepsilon_y \\ \gamma_{xy} \end{bmatrix} = \sigma_x \begin{bmatrix} \bar{S}_{11} \\ \bar{S}_{12} \\ \bar{S}_{16} \end{bmatrix} \tag{9.2}$$

Consequently, the off-axis coupon subjected to a uniform uniaxial state of stress thus exhibits shear strain (γ_{xy}) in addition to the axial and transverse strains (ε_x and ε_y) (Figure 9.2).

A set of material properties may be evaluated based on measurement of axial stress (σ_x) and axial, transverse, and shear strains (ε_x, ε_y, γ_{xy}). It is customary to determine the axial Young's modulus (E_x) and Poisson's ratio (ν_{xy}) of the off-axis specimen

$$E_x = \frac{\sigma_x}{\varepsilon_x} \tag{9.3}$$

$$\nu_{xy} = -\frac{\varepsilon_y}{\varepsilon_x} \tag{9.4}$$

In addition, a ratio (η_{xy}), which quantifies coupling between shear and axial strains, is defined according to

$$\eta_{xy} = \frac{\gamma_{xy}}{\varepsilon_x} \tag{9.5}$$

The off-axis tension test may also be used to determine the in-plane shear modulus, G_{12}, in the principal material coordinate system. This property is, according to Equation (2.9), defined by

$$G_{12} = \frac{\tau_{12}}{\gamma_{12}} \tag{9.6}$$

Consequently, determination of G_{12} requires determination of shear stress and strain in the principal material coordinate system. Equations (2.12) and (2.14) yield

$$\tau_{12} = -mn\sigma_x \tag{9.7}$$

where $m = \cos\theta$ and $n = \sin\theta$. The shear strain is obtained from Equations (2.14)

$$\gamma_{12} = 2mn(\varepsilon_y - \varepsilon_x) + (m^2 - n^2)\gamma_{xy} \tag{9.8}$$

where the strain (ε_x) is directly measured, and the transverse strain (ε_y) and shear strain (γ_{xy}) are determined as subsequently explained.

The properties E_x, ν_{xy}, η_{xy}, and G_{12} can be evaluated from test data using procedures detailed later in this chapter. The mechanical properties so determined can be compared to theoretical values calculated from the compliance relations, Equations (9.2), and the definitions in Equations (9.3–9.5),

$$E_x = \frac{1}{\bar{S}_{11}} \tag{9.9a}$$

$$\nu_{xy} = \frac{-\bar{S}_{12}}{\bar{S}_{11}} \tag{9.9b}$$

$$\eta_{xy} = \frac{\bar{S}_{16}}{\bar{S}_{11}} \tag{9.9c}$$

If the principal (basic) material properties (E_1, E_2, ν_{12}, and G_{12}) are known from previous tests (Chapters 5–7), it is possible to calculate the off-axis properties E_x, ν_{xy}, and η_{xy} using Equations (A.1) (Appendix A), and compare those to the experimentally determined values. G_{12} may be compared to the modulus measured in the off-axis test (Equation (9.6)).

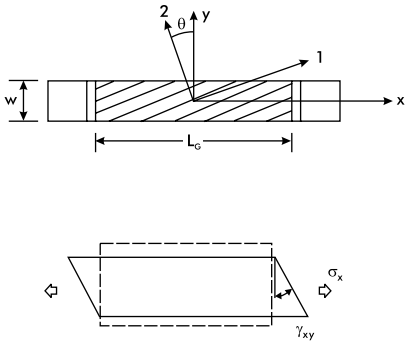

FIGURE 9.2
Off-axis coupon under uniform axial stress.

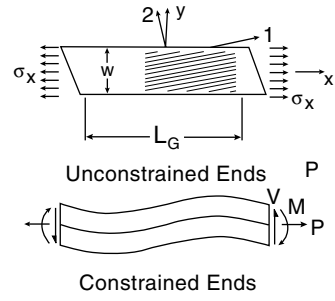

FIGURE 9.3
Influence of gripped end regions on deformation of off-axis specimen [2].

9.2 Influence of End Constraint

As first pointed out by Halpin and Pagano [2], most test machines used in testing laboratories employ rigid grips that constrain the shear deformation illustrated in Figure 9.2. As a result, the specimen assumes a shape schematically illustrated in Figure 9.3 [2]. To quantify the influence of gripping on the response of an off-axis tension specimen, Halpin and Pagano [2] performed a stress analysis of a constrained coupon and obtained the following expressions for the shear strain and longitudinal strain at the specimen centerline.

$$\gamma_{xy} = \bar{S}_{16} C_2 - \bar{S}_{66} C_0 w^2 / 4 \tag{9.10a}$$

$$\varepsilon_x = \bar{S}_{11} C_2 - \bar{S}_{16} C_0 w^2 / 4 \tag{9.10b}$$

with

$$C_0 = \frac{12\bar{S}_{16}\varepsilon_0}{3w^2\left(\bar{S}_{11}\bar{S}_{66} - \bar{S}_{16}^2\right) + 2\bar{S}_{11}L_G^2} \tag{9.11a}$$

$$C_2 = \frac{C_0}{12\bar{S}_{16}}\left(3\bar{S}_{66}w^2 + \bar{S}_{11}L_G^2\right) \tag{9.11b}$$

where $\varepsilon_0 = \Delta L / L_G$ (elongation/gage length) and w and L_G are specimen width and gage length, respectively (Figure 9.1).

On the basis of this analysis, it is possible to derive an expression for the apparent axial Young's modulus including end constraint

$$(E_x)_a = \sigma_x/\varepsilon_x \tag{9.12}$$

where σ_x and ε_x are the stress and strain at the centerline of the constrained off-axis coupon. $(E_x)_a$ may be expressed as

$$\left(E_x\right)_a = \frac{E_x}{1-\xi} \tag{9.13}$$

in which E_x is the modulus for an unconstrained off-axis specimen. The parameter ξ is given by

$$\xi = \frac{1}{\bar{S}_{11}}\left[\frac{3\bar{S}_{16}^2}{3\bar{S}_{66}+2\bar{S}_{11}\left(L_G/w\right)^2}\right] \tag{9.14}$$

Examination of the above equations reveals that $\xi \to 0$ and $(E_x)_a \to E_x = 1/\bar{S}_{11}$ when $L_G/w \to \infty$.

Similarly, Pindera and Herakovich [3] derived an expression for the apparent Poisson's ratio, $(\nu_{xy})_a$

$$\left(\nu_{xy}\right)_a = \nu_{xy}\,\frac{1-\frac{3}{2}\left(\frac{\bar{S}_{26}}{\bar{S}_{11}}\right)\beta}{1-\frac{3}{2}\left(\frac{\bar{S}_{16}}{\bar{S}_{12}}\right)\beta} \tag{9.15}$$

where β is given by [3],

$$\beta = \frac{\left(\frac{w}{L_G}\right)^2\left(\frac{\bar{S}_{16}}{\bar{S}_{11}}\right)}{1+\frac{3}{2}\left(\frac{w}{L_G}\right)^2\left(\frac{\bar{S}_{66}}{\bar{S}_{11}}\right)} \tag{9.16}$$

The apparent shear coupling ratio of the specimen subjected to end constraint is

$$(\eta_{xy})_a = \gamma_{xy}/\varepsilon_x \tag{9.17}$$

Substitution of Equations (9.10) and (9.11) into (9.17) yields

$$\left(\eta_{xy}\right)_a = \frac{\bar{S}_{16}}{\bar{S}_{11}}\left[1+\frac{3}{2}\left(\frac{w}{L_G}\right)^2\left(\frac{\bar{S}_{66}}{\bar{S}_{11}}-\left(\frac{\bar{S}_{16}}{\bar{S}_{11}}\right)^2\right)\right]^{-1} \tag{9.18}$$

Note that when the length-to-width ratio, $L_G/w \to \infty$, $(\eta_{xy})_a \to \bar{S}_{16}/\bar{S}_{11}$, as given by Equation (9.9c).

Pindera and Herakovich [3] examined the influence of end constraint on the evaluation of shear modulus, G_{12}, from the off-axis tension specimen using the elasticity solution of Halpin and Pagano [2] and found that the procedure outlined in Section 9.1 leads to error in G_{12}. The main source of error is the neglect of the shear stress τ_{xy} in Equation (9.7). The proper transformation is [3]

$$\tau_{12} = -mn\sigma_x + (m^2 - n^2)\tau_{xy} \tag{9.19}$$

This equation, combined with the definition of G_{12} (Equation (9.6)), yields an expression for the correct value of the shear modulus in terms of the apparent modulus $(G_{12})_a$, evaluated using the procedure in Section 9.1 [3],

$$G_{12} = \left(G_{12}\right)_a \frac{1+\dfrac{3\left(m^2-n^2\right)}{2mn}\beta}{1-\beta\left(\bar{S}_{16}/\bar{S}_{11}\right)} \tag{9.20}$$

where $m = \cos\theta$, $n = \sin\theta$, and β is defined in Equation (9.16). As $(w/L_G) \to \infty$, $\beta \to 0$, and the apparent shear modulus approaches G_{12}.

The above expressions for apparent off-axis properties $(E_x)_a$, $(\nu_{xy})_a$, and $(\eta_{xy})_a$ may be used to correct measured values, or to design the off-axis specimen for minimum error resulting from end constraint. An obvious way to reduce the error is to use specimens with large aspect ratios, L_G/w. As mentioned early in this chapter, specimens are typically 230 mm long and between 12.7 and 25.4 mm wide. For 38-mm-long tabs at the ends, this corresponds to aspect ratios between 6 and 12. For a carbon/polyimide composite specimen with an aspect ratio of 10 and 10° off-axis angle, Pindera and Herakovich [3] found an error in E_x of about 2 to 4%. The error in shear coupling ratio is larger, as will be discussed later.

The error in shear modulus G_{12} for a 10° off-axis carbon/polyimide specimen at $L_G/w = 10$ is approximately 12 to 15% [3]. For proper determination of G_{12}, Pindera and Herakovich [3] recommend use of coupons with an aspect ratio of 10 or more and an off-axis angle of 45°.

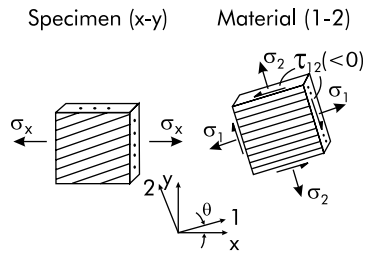

FIGURE 9.4
State of stress in the specimen for an off-axis tension test.

9.3 Off-Axis Tensile Strength

As mentioned earlier in this chapter, the off-axis tension test has been used to examine theories proposed for prediction failure of composites under combined stress. In such studies, slender specimens are used for strength measurements to avoid the complications of end constraint effects discussed above. This leads to a stress state in the on-axis system, as given by Equations (2.12) and (2.14):

$$\begin{bmatrix} \sigma_1 \\ \sigma_2 \\ \tau_{12} \end{bmatrix} = \sigma_x \begin{bmatrix} m^2 \\ n^2 \\ -mn \end{bmatrix} \tag{9.21}$$

Therefore, as illustrated in Figure 9.4, the state of stress in the principal material coordinate system is biaxial.

Experimental studies conducted on on-axis and off-axis specimens, e.g., in References [4,5], show that the off-axis specimen under tension fails along planes parallel to the fibers except for zero and very small angles, where failure involves fiber fractures. To predict the failure stress of the off-axis tension specimen, the on-axis stresses given by Equations (9.21) are substituted into the failure criterion of choice (see Section 2.5). The maximum stress and strain criteria (see Section 2.5), yield three equations for the ultimate stress, σ_x^{ult}, and the appropriate strength is identified by the least of the three values. Substitution of the stresses given by Equations (9.21) into the Tsai-Wu criterion, Equation (2.44), yields a quadratic equation in σ_x^{ult}, of the type

$$A\left(\sigma_x^{ult}\right)^2 + B\sigma_x^{ult} - 1 = 0 \tag{9.22}$$

The solution of Equation (9.22) yields two roots, the positive associated with the tensile strength and the negative associated with the compressive strength of the off-axis specimen.

As mentioned early in this chapter, the 10° off-axis tension test has been proposed for measuring the in-plane shear strength (S_6) of unidirectional composites [1]. However, because failure occurs under the influence of normal stresses σ_1 and σ_2 (Figure 9.4), which separate the specimen in two pieces, this test is not recommended for the generation of shear strength [6].

9.4 Test Procedure

1. Prepare off-axis tension coupons from a unidirectional, six- to eight-ply-thick panel. The specimens should be about 230 mm long and between 12.5 and 25 mm wide. Select at least three different off-axis angles, e.g., 15, 30, and 60°. Use the same tolerances as for the tension specimen discussed in Chapter 5, and bond end tabs as described in Chapter 4.
2. The off-axis test specimen is instrumented with a three-element strain gage rosette with one of the elements aligned with the coupon axis (x-direction in Figure 9.1), one element at 45°, and one element at –45°.
3. Measure the specimen cross-sectional dimensions (average six measurements).
4. Mount the specimen in a properly aligned and calibrated test frame. Set the crosshead rate at about 0.5 to 1 mm/min.
5. Monitor the load-strain response of the specimen (all three elements). Take strain readings at small load intervals to collect at least 25 data points in the linear region. Load the specimen to failure.

9.5 Data Reduction

9.5.1 Elastic Properties

Axial modulus, Poisson's ratio and shear coupling ratio may be determined from measured stress-strain data according to Equations (9.3)-(9.5). The axial strain, ε_x, is obtained directly from the axially oriented strain gage. Transverse strain and shear strain, ε_y and γ_{xy}, are obtained from the ±45° gages using Equations (2.13).

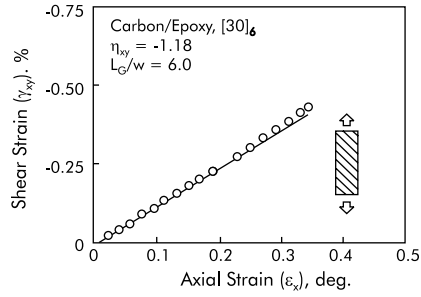

FIGURE 9.5
Shear strain vs. axial strain for a $[30]_6$ carbon/epoxy composite.

$$\varepsilon(45°) = (\varepsilon_x + \varepsilon_y + \gamma_{xy})/2 \tag{9.23a}$$

$$\varepsilon(-45°) = (\varepsilon_x + \varepsilon_y - \gamma_{xy})/2 \tag{9.23b}$$

Combining Equations (9.23) yields

$$\varepsilon_y = \varepsilon(45°) + \varepsilon(-45°) - \varepsilon_x \tag{9.24}$$

$$\gamma_{xy} = \varepsilon(45°) + \varepsilon(-45°) \tag{9.25}$$

Young's modulus, E_x, is determined from the initial slope of the curve σ_x vs. ε_x. Poisson's ratio, ν_{xy}, is obtained by plotting the negative of the strain ε_y vs. ε_x and determining the slope of the line. The shear coupling ratio, η_{xy}, is determined by plotting shear strain vs. axial strain, as shown in Figure 9.5 for a 30° off-axis carbon/epoxy specimen. Note that the experimentally determined properties are apparent because they may be influenced by the constraints imposed by the grips.

Figures 9.6–9.8 show experimentally obtained off-axis modulus, Poisson's ratio, and shear coupling ratio vs. off-axis angle for carbon/fiber composites. Shown in these graphs are reduced data (apparent), theoretical curves calculated assuming the ends of the specimen are free to rotate (Equations (9.9)), and theoretical curves calculated using a correction for end constraint according to Section 9.2. It is observed that the apparent modulus and Poisson's ratio are larger than the unconstrained value, whereas the magnitude of the apparent shear coupling ratio is reduced because of end constraints. The expressions in Section 9.2 incorporating end constraints due to finite aspect ratio bring the analytical results in close agreement with measured data.

The apparent shear modulus, G_{12}, determined for a carbon/polyimide composite using Equations (9.6) – (9.8) and corrected for shear stress and end constraint using Equation (9.20), is shown vs. off-axis angle in Figure 9.9. At off-axis angles up to 30° the end constraint will increase the apparent

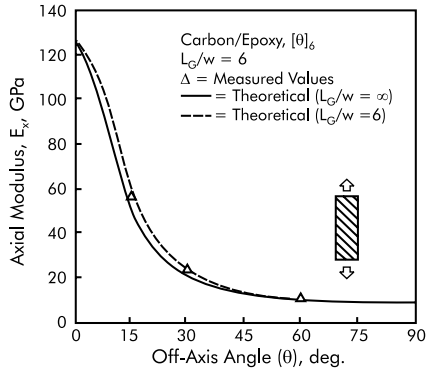

FIGURE 9.6
Axial modulus vs. off-axis angle for a carbon/epoxy composite.

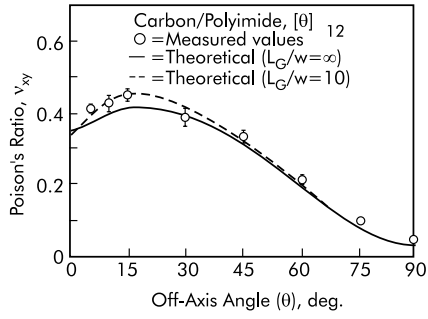

FIGURE 9.7
Poisson's ratio vs. off-axis angle for a carbon/polyimide composite.

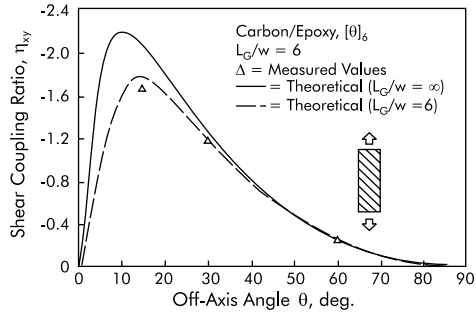

FIGURE 9.8
Shear coupling ratio vs. off-axis angle for a carbon/epoxy composite.

modulus. Correction of the apparent shear modulus for end constraint brings the value closer to the asymptotic value. This graph emphasizes the need to use off-axis specimens of angles 45° or greater when evaluating the shear modulus.

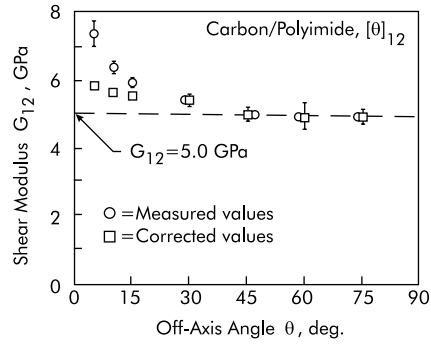

FIGURE 9.9
Shear modulus vs. off-axis angle for a carbon/polyimide composite [3].

TABLE 9.1

Basic Ply Mechanical Properties for Carbon/Epoxy and Carbon/Polyimide Composites Considered in Figures 9.5–9.10

Material	E_1 (GPa)	E_2 (GPa)	ν_{12}	G_{12} (GPa)
Carbon/epoxy	126	10.0	0.30	5.2
Carbon/polyimide [3]	137	9.79	0.35	5.0

As a reference, basic ply properties for the carbon/epoxy and carbon/polyimide composites considered are listed in Table 9.1.

9.5.2 Tensile Strength of Off-Axis Specimen

Table 9.2 presents off-axis tensile strength data for the carbon–epoxy composite. Figure 9.10 shows experimentally determined failure stress vs. off-axis angle for a carbon/epoxy composite (Table 9.2). Excellent agreement is noted.

TABLE 9.2

Off-Axis Strength Data for a Carbon/Epoxy Composite

Angle, θ (degrees)	Tensile Strength (MPa)
5	780
15	305
30	112
60	65

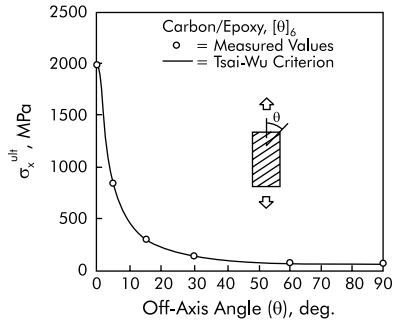

FIGURE 9.10
Tensile failure stress vs. off-axis angle for a carbon/epoxy composite.

References

1. C.C. Chamis and J.H. Sinclair, Ten-degree off-axis test for shear properties in fiber composites, *Exp. Mech.*, 17, 339–346, 1977.
2. J.C. Halpin and N.J. Pagano, Influence of end constraint in the testing of anisotropic bodies, *J. Compos. Mater.*, 2, 18–31, 1968.
3. M.J. Pindera and C.T. Herakovich, Shear characterization of unidirectional composites with the off-axis tension test, *Exp. Mech.*, 26, 103–112, 1986.
4. R.B. Pipes and B.W. Cole, On the off-axis strength test of anisotropic materials, *J. Compos. Mater.*, 7, 246–256, 1973.
5. M.J. Pindera and C.T. Herakovich, *An Endochronic Theory for Transversely Isotropic Fibrous Composites*, Report VPI-E-81-27, Virginia Polytechnic Institute and State University, Blacksburg, VA, 1981.
6. S. Chatterjee, D.F. Adams, and D.W. Oplinger, *Test Methods for Composites — A Status Report*, Vol. III., Shear Test Methods, DOT/FAA/CT-93/17 III, FAA Technical Center, Atlantic City International Airport, NJ, June 1993.